

# Long bed waves in tidal seas: an idealized model

PAOLO BLONDEAUX<sup>1</sup>†, HUIB E. DE SWART<sup>2</sup>  
AND GIOVANNA VITTORI<sup>1</sup>

<sup>1</sup>Department of Civil, Environmental and Architectural Engineering, Genoa University,  
Via Montallegro 1, 16145 Genova, Italy

<sup>2</sup>Institute for Marine and Atmospheric Research, Utrecht University, Princetonplein 5,  
3584 CC Utrecht, The Netherlands

(Received 19 March 2009; revised 23 June 2009; accepted 23 June 2009)

An idealized model is proposed to explain the appearance of the long bed waves that have been recently observed in shallow tidal seas. The model assumes that these bedforms grow due to tide–topography interaction. The water motion is described by means of the depth-averaged shallow water equations and the bottom evolution is governed by conservation of sediment mass. The sediment transport formulation includes a critical bottom stress below which no sediment moves. Also, anisotropic sediment transport, due to local bottom slopes in the longitudinal and transverse directions, is taken into account. A linear stability analysis of the flat bottom configuration reveals that different bottom patterns can emerge. In accordance with previous analyses, for strong tidal currents, the fastest growing modes are sand banks. However, if the tidal currents are elliptical and the maximum bottom stress is just above its threshold value for the initiation of sediment motion, the model shows the presence of further growing modes which resemble the long bed waves observed in the field.

---

## 1. Introduction

Two types of offshore periodic bottom forms are often observed in shallow seas and are usually linked to oscillatory tidal currents. The first are sand waves, which have wavelengths of a few hundreds of metres and crests almost orthogonal to the major axis of the local depth-averaged tidal ellipse. The second are sand banks, which have much longer wavelengths ( $O(10\text{ km})$ ) and crests that make a small angle with the tidal current.

By analysing bathymetric surveys made in the North Sea, Knaapen *et al.* (2001) have identified new bedforms which can be classified neither as sand waves nor as sand banks. These new bedforms, named long bed waves, are characterized by crests which are  $60^\circ$  counterclockwise rotated with respect to the direction of the tidal current and by a wavelength of about 1.6 km. A further analysis of the bathymetric data of the south-western part of the Dutch continental shelf (Van Dijk, 2008, private communication) reveals the spatial extent of long bed waves and shows that these bedforms are both clockwise and counterclockwise rotated with respect to the major axis of the tidal current ellipse (see figure 1). The clockwise bedforms form an angle of about  $33^\circ$ , while the counterclockwise bedforms form an angle of about  $64^\circ$  with respect to the tidal ellipse. The large-scale grey patches in figure 1 represent

† Email address for correspondence: blx@dicat.unige.it

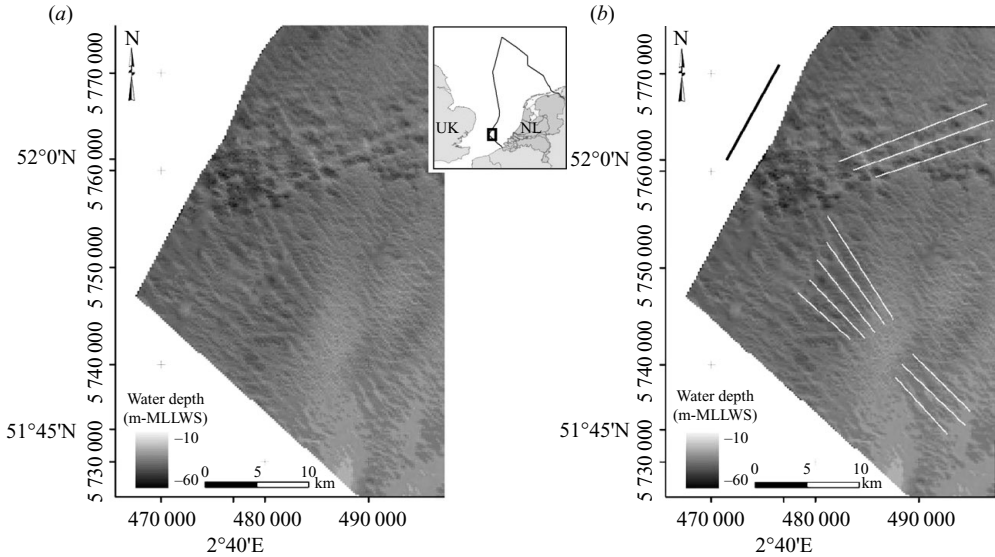


FIGURE 1. Bathymetry of the surveyed area at the offshore end of the access channel to Rotterdam harbour. The position of the surveyed area is sketched at the top-right corner of (a). The bathymetric data are provided by TNO (Netherlands Organization for Applied Scientific Research) and are compiled from measurements of the Netherlands Hydrographic Office of the Royal Netherlands Navy (courtesy of T. Van Dijk). Some of the crests of the long bed waves observed in the area are marked by white lines on (b) where the black line at the top-left corner indicates the orientation of the major axis of the tidal ellipse.

counterclockwise rotated sand banks of small amplitude, as recently described by Knaapen (2008). Moreover, sand waves occur throughout the entire area. Process-based models, able to explain and simulate the excitation of tidal sand banks and sand waves, are already available (a.o. the first contributions of Richards 1980; Huthnance 1982; Hulscher, De Swart & De Vriend 1993 and the recent unified approach of Besio, Blondeaux & Vittori 2006). These bedforms emerge as free instabilities of a state that constitutes tidal flow over a flat bottom. However, a model able to describe the formation of long bed waves is still missing. In the following, it is shown that the appearance of long bed waves can be explained by means of a simple model, similar to that used to investigate the formation of sand banks. In §2, we briefly summarize the hydrodynamic and morphodynamic models used to determine the time development of the bottom configuration of shallow tidal seas. The flow and sediment transport generated by tidal currents over a flat bottom are described in §3, along with the investigation of the stability of the flat-bed configuration. The results of the stability analysis are described in §4, where also a comparison of the theoretical findings with field observations is made. Moreover, in §4, the sensitivity of the results to changes of the model parameters is discussed. Finally, the conclusions are drawn in §5.

## 2. Formulation of the problem

A shallow sea of depth  $h^*$  is considered and a Cartesian coordinate system is introduced such that the  $x^*$ - and  $y^*$ -axis lie on the undisturbed free surface and the  $z^*$ -axis is vertical, pointing upwards (hereinafter a star denotes dimensional quantities and the same symbol without the star denotes their dimensionless counterpart). The water is assumed to have a constant density  $\rho^*$  and the seabed is composed of a

cohesionless sediment of uniform size  $d^*$  and density  $\rho_s^*$ . The water and sediment motions are driven by free surface gradients of tidal origin which oscillate in time with an angular frequency  $\omega^*$ . The average water depth and the maximum value of the depth-averaged velocity during the tidal cycle are denoted by  $h_0^*$  and  $U_0^*$ , respectively. By using the  $f$ -plane approximation, the problem of flow determination is posed by continuity and momentum equations, where the Coriolis contribution related to the Earth's rotation should be taken into account because it affects the tidal current. Since the water depth turns out to be much smaller than the horizontal scale of the problem (the wavelength of the bottom forms), the shallow water approximation is introduced and depth-averaged values of the velocity components are considered. The problem can be simplified by assuming that both the Froude number  $F$  of the tide ( $F = U_0^*/\sqrt{g^*h_0^*}$ ,  $g^*$  being the gravitational acceleration) and the ratio  $\beta$  between the tidal period and the morphodynamic time scale (to be defined later on) are much smaller than 1. The assumption  $F \ll 1$  allows the rigid lid approximation to be introduced, while the assumption  $\beta \ll 1$  allows the time derivative of the water depth to be neglected in fluid continuity equation. Equations of motion will be given in terms of the dimensionless variables

$$(x, y) = \frac{(x^*, y^*)}{U_0^*/\omega^*}, \quad t = t^*\omega^*, \quad (U, V) = \frac{(U^*, V^*)}{U_0^*}, \quad h = \frac{h^*}{h_0^*}. \quad (2.1)$$

Here,  $t^*$  is time and  $(U^*, V^*)$  are the depth-averaged velocity components along the  $x^*$ - and  $y^*$ -axis, respectively. The continuity and momentum equations read

$$\frac{\partial(hU)}{\partial x} + \frac{\partial(hV)}{\partial y} = 0, \quad (2.2)$$

$$\frac{\partial(U, V)}{\partial t} + U \frac{\partial(U, V)}{\partial x} + V \frac{\partial(U, V)}{\partial y} = -(E_x, E_y) - \mu \frac{C_0^2(U, V)\sqrt{U^2 + V^2}}{C^2 h} + f(V, -U), \quad (2.3)$$

where  $(E_x, E_y)$  are the free surface gradient components which drive the tidal current and are of order one, being scaled with  $U_0^*\omega^*/g^*$ . The second term on the right-hand side is the dimensional frictional force per mass unit, which is the ratio of the bed shear stress and the depth. A nonlinear constitutive relationship is used to relate the dimensional bed shear stress to the velocity field,

$$(\tau_x^*, \tau_y^*) = \rho^* U_0^{*2} \frac{(U, V)\sqrt{U^2 + V^2}}{C^2}. \quad (2.4)$$

Hereinafter, the parameter  $C = C_z/\sqrt{g^*}$ ,  $C_z$  being the Chézy coefficient, is called the conductance coefficient. A standard formula is used to express  $C$  in terms of the dimensionless roughness  $z_r = z_r^*/h_0^*$  of the sea bottom ( $C = 2.5 \ln(11h/z_r)$ ) and the value of  $C_0$  is that of  $C$  evaluated for  $h = 1$ . By assuming that the bottom roughness is mainly due to the presence of small scale bottom forms (ripples), the value of  $z_r^*$  is set equal to the ripple height, which can be determined using the predictors of Soulsby (1997) and Soulsby & Whitehouse (2005). In (2.2) and (2.3) two further dimensionless parameters appear:

$$\mu = \frac{U_0^*}{C_0^2 \omega^* h_0^*}, \quad f = 2 \frac{\Omega^*}{\omega^*} \sin \Phi. \quad (2.5)$$

The parameter  $\mu$  represents the ratio of the tidal period and the frictional time scale. Furthermore,  $f$  is the Coriolis parameter, with  $\Omega^*$  the angular velocity of the Earth's rotation and  $\Phi$  the local latitude.

The evolution of the seabed is governed by the sediment continuity equation, which states that the convergence (or divergence) of the sediment transport causes a rise (or fall) of the bed level. By introducing the dimensionless sediment transport rates

$$(\overline{Q}_x, \overline{Q}_y) = \frac{(Q_x^*, Q_y^*)}{[Q^*]}, \quad (2.6)$$

with  $(Q_x^*, Q_y^*)$  the  $x^*$  and  $y^*$  components of the volumetric sediment transport rate per unit width, the sediment continuity equation can be written in the form

$$\frac{\partial h}{\partial t} = \beta \left[ \frac{\partial \overline{Q}_x}{\partial x} + \frac{\partial \overline{Q}_y}{\partial y} \right]. \quad (2.7)$$

Here,  $\beta = [Q^*]/((1-n)U_0^*h_0^*)$  is the ratio between the tidal period and the morphodynamic time scale,  $n$  being the porosity of the bottom material. In principle, the sediment transport rate scales with the magnitude of the bottom stress. However, for typical field conditions, the choice  $[Q^*] = \sqrt{(\rho_s^*/\rho^* - 1)g^*d^{*3}}$  yields a good estimate of the transport rate, as it follows from the empirical predictors commonly encountered in the literature.

Since  $\beta \ll 1$ , significant changes of the bottom configuration only occur after a large number of tidal cycles. Hence, it is convenient to introduce a new time variable  $T = \beta t$  and to assume that the bed profile is a function of  $t$  and  $T$ . The dependence of  $h$  on  $t$  describes the small ( $O(\beta)$ ) oscillations of the bottom taking place during the tidal cycle, while the dependence of  $h$  on  $T$  describes the slow but significant growth/decay of  $h$  taking place on the morphodynamic time scale. The fact that  $\beta \ll 1$  implies that the oscillations of the bottom on the tidal time scale have a negligible influence on the evolution of the bed on the morphodynamic time scale. Consequently, (2.7) can be replaced by

$$\frac{\partial h}{\partial T} = \frac{\partial \overline{Q}_x}{\partial x} + \frac{\partial \overline{Q}_y}{\partial y}, \quad (2.8)$$

$(\overline{Q}_x, \overline{Q}_y)$  being the sediment transport rate averaged over the tidal period.

To evaluate the sediment transport rate, the suspended load is assumed to be negligible. This means that turbulent eddies, being generated by tidal currents, are unable to pick up the sediment particles from the bottom and carry them into suspension. The formulation of Fredsøe & Deigaard (1992) is used to quantify the bed load. The latter depends on the  $x$  and  $y$  components of the dimensionless skin friction  $(\theta_x, \theta_y)$ :

$$(\theta_x, \theta_y) = \frac{(\tau_x'^*, \tau_y'^*)}{(\rho_s^* - \rho^*)g^*d^*}. \quad (2.9)$$

The components of  $(\tau_x'^*, \tau_y'^*)$  are evaluated from (2.4) by replacing  $C$  with the conductance coefficient due to the sediment grains  $C_d$ , i.e.  $C_d = 2.5 \ln(11h_0^*/(2.5d^*))$ . Finally, following Kovacs & Parker (1994), a contribution to the sediment transport formulation by Fredsøe & Deigaard (1992) is added to take into account that the sediment is transported easier downhill than uphill. The result is

$$(\overline{Q}_x, \overline{Q}_y) = \frac{30}{\mu_d \pi} (\theta - \theta_c) (\sqrt{\theta} - 0.7\sqrt{\theta_c}) \left[ \frac{(\theta_x, \theta_y)}{\theta} + \left( \frac{\partial h}{\partial x}, \frac{\partial h}{\partial y} \right) \mathbf{G} \frac{\omega^* h_0^*}{U_0^*} \right] \mathcal{H}(\theta - \theta_c). \quad (2.10)$$

In (2.10),  $\theta$  is equal to  $\sqrt{\theta_x^2 + \theta_y^2}$ ,  $\theta_c$  is the critical value of the Shields parameter such that for  $\theta$  smaller than  $\theta_c$  no sediment moves, and  $\mathcal{H}$  is the Heaviside function. The value of  $\theta_c$  is fixed at 0.05. Experimental observations of various authors (a.o. Talmon, Struiksma & Van Mierlo 1995) provide estimates for the values of the components of the tensor  $\mathbf{G}$  (Seminara 1998). Using a reference frame  $(s, n)$  such that  $s$  is aligned with the bed shear stress, it turns out that

$$G_{ns} = G_{sn} = 0, \quad G_{ss} = \frac{\theta_c}{\mu_d} \frac{1}{\mathcal{Q}} \frac{d\mathcal{Q}}{d\theta}, \quad G_{nn} = \frac{k_G}{\sqrt{\theta}}, \quad (2.11)$$

where  $\mathcal{Q}$  is the modulus of the sediment transport rate over a flat bed,  $\mu_d$  is the dynamic friction coefficient of the bed material and  $k_G$  is a coefficient.

The present depth-averaged model for offshore tidal bedforms differs from earlier models (cf. Huthnance 1982). First, the conductance coefficient  $C$  is not constant, since it depends on the local water depth. Second, a more sophisticated sediment transport formulation is used, which includes a critical shear stress for erosion and a slope induced anisotropic sediment transport.

### 3. The growth of the bottom forms

As in many other morphodynamic models, the bottom features are assumed to emerge as inherent instabilities of a simple basic state of the coupled water-bottom system. The present model allows for a basic state which is characterized by a flat horizontal bed and a spatially uniform velocity field, i.e.  $(U, V) = (U_0(t), V_0(t))$  and  $h = 1$ . In particular, (2.8)–(2.10) show that this is a morphodynamic equilibrium state. Next, the stability properties of this basic state are investigated by adding a bottom perturbation of small amplitude and investigating the growth or decay of this perturbation. Since the perturbation is assumed to have a small amplitude, the problem is linearized and the bottom profile is described by the superposition of different spatial components, which, in the linear regime, evolve independently of each other. Hence, the problem can be solved for the generic spatial component of the bottom configuration. Here, the  $x$ -axis is chosen to be aligned with the crests of the bottom form so, without loss of generality, we consider a bottom profile described by

$$h = 1 - \epsilon [A(T)e^{iky} + c.c.]. \quad (3.1)$$

In (3.1)  $\epsilon A(T)$  is the amplitude of the generic component which is periodic in the  $y$  direction with an arbitrary wavenumber  $k$ . Moreover,  $c.c.$  indicates the complex conjugate of the previous term. The parameter  $\epsilon$  is assumed to be much smaller than 1 and  $A(T)$  is a function of the morphodynamic time coordinate  $T$ , which describes the growth/decay of the bottom perturbation. The small value of  $\epsilon$  allows the solution to be expanded in the form

$$(U, V, E_x, E_y, C) = (U_0, V_0, E_{x0}, E_{y0}, C_0) + \epsilon [(U_1, V_1, 0, E_{y1}, C_1)A(T)e^{iky} + c.c.] + O(\epsilon^2), \quad (3.2)$$

with  $C_0 = 2.5 \ln(11/z_r)$  and  $C_1 = -2.5$ . At the leading order, i.e.  $O(\epsilon^0)$ , the solution as described above is obtained. At order  $\epsilon$ , fluid continuity equation yields

$$V_1 = V_0. \quad (3.3)$$

Substitution of (3.3) into the linearized momentum equation along the  $x$ -axis results in

$$\frac{dU_1}{dt} = -ikV_0U_1 + fV_0 - \mu\sqrt{U_0^2 + V_0^2} \left[ U_1 \left( 1 + \frac{U_0^2}{U_0^2 + V_0^2} \right) + U_0 \left( 1 + \frac{V_0^2}{U_0^2 + V_0^2} + \frac{5}{C_0} \right) \right]. \quad (3.4)$$

The interest is in the non-transient part of the solution  $U_1$  of (3.4), which is determined by standard numerical methods. Finally, the linearized version of the  $y$  component of (2.3) is used to determine  $E_{y1}$ , even though  $E_{y1}$  is not necessary to obtain the time development of the bottom perturbation.

Once the hydrodynamic problem is solved, the amplitude equation, which provides the time development of the amplitude  $A(T)$  of the generic component of the bottom perturbation, follows from sediment continuity equation. The result is

$$\frac{dA(T)}{dT} = -ik\overline{Q}_{y1}A(T) = \Gamma A(T), \quad (3.5)$$

where the variable  $\overline{Q}_{y1}$ , which is the time average of the contribution of order  $\epsilon$  to  $Q_y$ , follows from (2.10). The solution of (3.5) is

$$A(T) = A_0 \exp[\Gamma T]. \quad (3.6)$$

The complex growth rate  $\Gamma$  depends on the parameters of the problem. Its real part  $\Gamma_r$  controls the growth/decay of the bottom perturbation, while its imaginary part equals  $-kc$ , where  $c$  is the migration speed of the perturbation.

In this study, we consider a basic state tidal flow that consists of a single tidal constituent and describes an elliptical tidal flow,

$$(U_0, V_0) = \sin(t) [\cos(\alpha), \sin(\alpha)] + e \cos(t) [\sin(\alpha), -\cos(\alpha)]. \quad (3.7)$$

Here,  $\alpha$  is the angle between the major axis of the tidal ellipse and the  $x$ -axis and  $e$  is the ratio between the minor and major axes of the tidal ellipse ( $-1 \leq e \leq 1$ ). Positive  $e$  refers to anticlockwise rotation of the tidal current vector, whilst negative  $e$  indicates clockwise rotation. Since this flow is symmetrical in time, the bedforms do not migrate and the imaginary part of  $\Gamma$  vanishes.

The growth rate can be determined for any value of the wavenumber  $k$  and the angle  $\alpha$ , given any fixed combination of the model parameters. The perturbation with the largest growth rate is called the fastest growing mode and is expected to dominate the solution after some time.

## 4. Results

### 4.1. Main findings

We consider values of the parameters representative of the coastal area shown in figure 1 and considered by Knaapen *et al.* (2001). The area is located at about  $52^\circ$  North and  $2^\circ 50'$  East. The sediment of the seabed is characterized by a mean grain size  $d^*$  equal to about 0.4 mm and the value of  $z_r^*$  can be set equal to 2.5 cm. The average water depth is 40 m and the dominant tide constituent is the semidiurnal component. According to numerical models of tide propagation in the North Sea (Carbajal 1997), the background depth-averaged tidal flow (i.e. the flow which is not affected by the bedforms) turns out to be characterized by a counterclockwise rotating velocity vector, with a maximum amplitude of about  $0.60 \text{ ms}^{-1}$ , which is not far from the critical value ( $\sim 0.58 \text{ ms}^{-1}$ ) for sediment erosion. The ratio  $e$  between

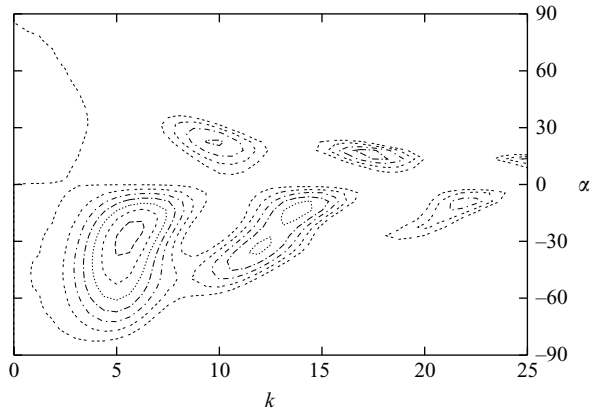


FIGURE 2. Dimensionless growth rate  $\Gamma_r$  of the bottom perturbations as function of their dimensionless wavenumber  $k$  and angle  $\alpha$  between their crests and the major axis of the tidal ellipse, for the default values of the parameters ( $\Delta\Gamma_r = 0.002$ , only positive values are displayed).

the minor and major axes of the tidal ellipse has a value of about 0.4. The values of the dimensionless parameters of the problem are  $f = 0.8$ ,  $\mu = 0.18$ ,  $z_r = 6.25 \cdot 10^{-4}$ ,  $d^*/h_0^* = 1.0 \cdot 10^{-5}$  and  $\beta = 2.2 \cdot 10^{-6}$ . Finally, following Seminara (1998), we choose  $\mu_d = 0.6$  and  $k_G = 0.55$ .

Figure 2 shows the growth rate  $\Gamma_r$  as function of  $k$  and  $\alpha$  for the values of the parameters given above. Note that  $k$  is the dimensionless wavenumber of the bottom perturbation, the crests of which are parallel to the  $x$ -axis, and  $\alpha$  is the angle between the major axis of the tidal ellipse and the crests of the bottom forms. Different relative maxima can be identified in figure 2. The maximum value of the growth rate is found for  $k = 5.6$  and  $\alpha = -27^\circ$ . This growing mode has a dimensional wavelength of about 4.8 km and its crests are counterclockwise rotated (angle of  $27^\circ$ ) with respect to the major axis of the tidal ellipse. This growing mode resembles the small amplitude tidal sand banks observed in the investigated area.

Two further relative maxima, each having a slightly smaller growth rate, can be identified in figure 2 for  $k$  equal to about 12.1 and 13.7 and  $\alpha$  equal to about  $-33^\circ$  and  $-14^\circ$ , respectively. These modes have crests that are counterclockwise rotated with respect to the major axis of the tidal ellipse and their wavelengths are approximately 2.2 km and 1.95 km, respectively. Both these modes have geometrical characteristics similar to those of the counterclockwise rotated long bed waves appearing in figure 1. In particular, their wavelength falls between those of sand waves and sand banks and agrees with the values measured in the field. The orientation of the modelled bedforms only qualitatively agrees with the observed values. A plausible reason for this discrepancy is that the present simple model does not account for different directions between depth-averaged tidal currents and tidal currents near the bottom. The latter in fact control the direction of the sediment transport.

Additional growing modes with positive values of  $\alpha$  can be recognized in figure 2. One is characterized by  $k = 9.8$  and  $\alpha = 22^\circ$ , the other by  $k = 17.4$  and  $\alpha = 16^\circ$ . Both these modes turn out to be clockwise rotated with respect to the major axis of the tidal ellipse and have dimensional wavelengths of about 2.7 km and 1.5 km, respectively. It is possible to correlate them with the long bed waves which appear to be clockwise rotated with respect to the direction of the tidal current, but again, their angle with

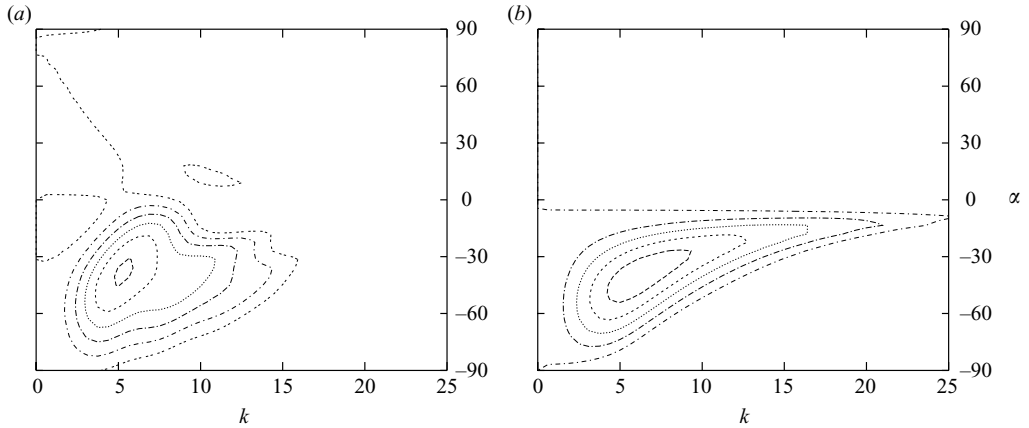


FIGURE 3. Dimensionless growth rate  $\Gamma_r$  of the bottom perturbations as function of their dimensionless wavenumber  $k$  and angle  $\alpha$  between their crests and the major axis of the tidal ellipse, for (a) the default values of the parameters but  $U_0^* = 0.90 \text{ ms}^{-1}$  and  $e = 0.4$  ( $\Delta\Gamma_r = 0.04$ , only positive values are displayed), (b) the default values of the parameters but  $U_0^* = 0.60 \text{ ms}^{-1}$  and  $e = 0$  ( $\Delta\Gamma_r = 0.002$ , only positive values are displayed).

the major axis of the tidal ellipse is smaller than that observed in the field. Note that the time evolution of the amplitude of the bottom forms is described by  $\exp(\Gamma\beta\omega^*t^*)$ . Taking into account the values of the parameters, for all the growing modes, the  $e$ -folding time turns out to be of  $O(10^3)$  years. However, close to the critical conditions for sediment erosion, the uncertainty of the sediment transport rate formulae is very large and the use of a different formula to quantify  $Q$  might lead to much larger sediment transport rates and to a reduction of the order of magnitude of the  $e$ -folding time. Moreover, as described in §4.2, for different values of the parameters, long bed waves grow at a much faster rate such that their  $e$ -folding time scale becomes of  $O(10^2)$  years.

Other growing modes can be identified in figure 2, but they have much smaller growth rates. The presence of multiple relative maxima and the emergence of long bed waves appear to be related to the relative weakness of the tidal current and to the ellipticity of the tidal current. Indeed, for the same values of the parameters as those of figure 2, but for stronger tidal velocities and/or unidirectional tidal currents, the amplification rate  $\Gamma_r$  has only one significant maximum which corresponds to sand banks. For example, figure 3(a) shows that, for  $U_0^* = 0.90 \text{ ms}^{-1}$ , the fastest growing mode has crests which are counterclockwise rotated with respect to the direction of the tidal current and a crest-to-crest distance of about 7.4 km. Similar conclusions apply with regard to the results shown in figure 3(b) (default values of the parameters but  $e = 0$ ).

In the case of strong tidal currents, as in figure 3(a), the mechanism that gives rise to the growth of the bottom forms is well known. The interaction of the oscillatory tidal current with ridges that are counterclockwise rotated with respect to the major axis of the tidal ellipse generates anticyclonic residual circulation cells around these ridges. The superposition of the basic tidal current and the steady current causes the velocity upstream of the crests slightly larger than the downstream velocity, at each phase of the tidal cycle. Since the amount of sediment transported by the current increases with increasing magnitude of the fluid velocity, the sediment is deposited at the crests and the amplitude of the ridges increases. In contrast, for clockwise

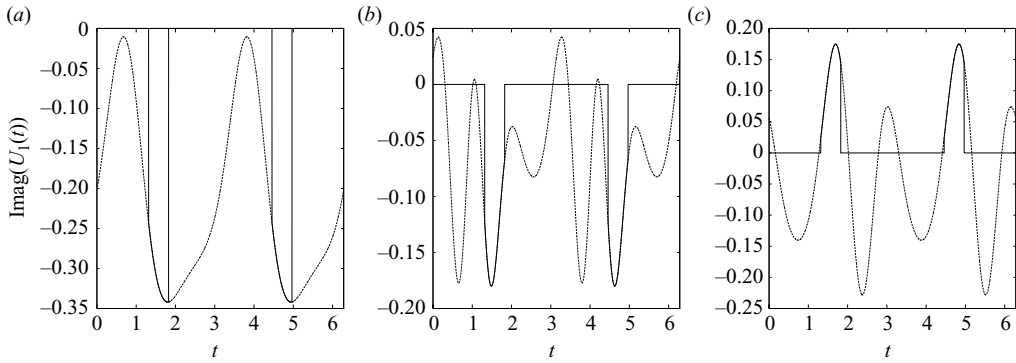


FIGURE 4. Imaginary part of the dimensionless, perturbed along-crest velocity component  $U_1$  versus dimensionless time during the tidal cycle (broken line) and considering only the phases such that  $\theta_0$  is larger than  $\theta_c$  (continuous line). The vertical lines in (a) indicate the phases at which  $\theta_0 = \theta_c$ , when the bed turns from active to passive, or viceversa. The horizontal solid lines in (b) and (c) indicate the stages during which the bed is not active. (a) 1st mode,  $k = 5.6$ ,  $\alpha = -27^\circ$ ; (b) 2nd mode,  $k = 12.1$ ,  $\alpha = -33^\circ$ ; (c) 4th mode,  $k = 9.8$ ,  $\alpha = 22^\circ$ .

rotated ridges, the velocity just upstream of the crests is slightly smaller than the downstream velocity. Consequently, the sediment is eroded from the crests and the amplitude of the bottom waviness decreases. For this reason, only the modes having negative values of  $\alpha$  tend to grow at a significant rate.

The physical explanation described above can be applied only if the seabed is active during the major part of the tidal cycle. In that case the mean sediment transport component  $\bar{Q}_{1y}$  is dominated by a contribution  $\sim \sin(2\alpha)\bar{U}_1$ . This can for instance be traced back from the original model of Huthnance (1982), which neglects the critical bottom stress in the sediment transport formulation. From (3.5) it then follows that the growth rate scales as  $\sim \sin(2\alpha)k \Im(\bar{U}_1)$ , where  $\Im$  denotes the imaginary part of a complex variable. Interestingly, it follows from sediment transport formulation (2.10) that also when tidal currents are weak, the largest contribution to  $\bar{Q}_{1y}$  is related  $\sim \sin(2\alpha)k \Im(\bar{U}_1)$ . Important here is that the average of the velocity field should be taken over the subintervals of the tidal cycle during which transport of sediment occurs ( $\theta > \theta_c$ ). This implies that growing bedforms with negative angles  $\alpha$  have a mean circulation, thus computed, which is anticyclonic around their crests ( $\Im(\bar{U}_1) < 0$ ). Likewise, growing bedforms with positive  $\alpha$  have cyclonic mean circulation around their crests, if the average is computed over the morphodynamically active part of the tidal cycle. This finding is confirmed by figure 4, which shows time series of  $\Im(\bar{U}_1)$  during one tidal period for three different bottom modes that were identified in the first experiment (figure 2). The solid line shows the value of  $\Im(\bar{U}_1)$  when  $\theta_0$  is larger than  $\theta_c$ . The residual flow calculated during the full tidal cycle differs considerably from that computed during the intervals that the bed is active. Indeed, the time averaged values of the imaginary part of  $U_1$  over the whole tidal period are  $-0.213, -0.068, -0.100, -0.033, -0.011$  for the first five modes, while the imaginary part of  $U_1$  averaged over the phases of the cycle with an active seabed are  $-0.051, -0.023, -0.032, 0.021, 0.022$ , respectively. Hence, both clockwise and counterclockwise rotated sand ridges can grow, giving rise to the clockwise and counterclockwise long bed waves which are observed in the field.

#### 4.2. Robustness of the results

We conclude the discussion of the results by pointing out that the model contains many parameters. The results previously described have been obtained by fixing those related to the site on the basis of the field measurements described in Knaapen *et al.* (2001) (namely the water depth  $h_0^*$  and the grain size  $d^*$ ) or on the basis of the results of numerical codes developed to describe the hydrodynamics of the investigated area (namely the tidal strength  $U_0^*$  and the eccentricity  $e$  of the tidal ellipse). Finally, the other parameters (the roughness size  $z_r^*$ , the dynamical friction coefficient  $\mu_d$ , the constant  $k_G$  ...) have been given values which are widely accepted in the literature. However, to ascertain the robustness of the model findings, further results have been obtained by halving and doubling the values of  $\mu_d$  and  $k_G$  and by considering values of  $z_r^*$  which are one-tenth and ten times the default value ( $z_r^* = 2.5$  cm). In all cases, the geometrical characteristics of the modelled bedforms (wavelength and orientation) do not significantly change. The largest variations of the wavelength and orientation of the five fastest growing modes are equal to 5%. However, it appears that for the smallest value of  $\mu_d$  ( $\mu_d = 0.3$ ) and the largest value of  $z_r^*$  ( $z_r^* = 25$  cm), the second mode merges into the third one. Vice versa, for the largest value of  $\mu_d$  ( $\mu_d = 1.2$ ), the third mode merges into the second one. Only the value of  $\mu_d$  appears to significantly affect the growth rate which increases/decreases by a factor 2 when  $\mu_d$  is halved/doubled. Runs have also been conducted for different values of the tidal strength  $U_0^*$  and eccentricity  $e$ . The model results show that, for  $e = 0.4$ , long bed waves appear when  $U_0^*$  is larger than the threshold value ( $0.58 \text{ ms}^{-1}$ ). For  $U_0^*$  larger than  $0.64 \text{ ms}^{-1}$ , only clockwise rotated long bed waves form and their growth rate becomes smaller as  $U_0^*$  is increased, but for  $U_0^*$  close to  $1 \text{ ms}^{-1}$  when counterclockwise rotated bed forms also appear with  $e$ -folding time scales of  $O(10^2)$  years. An  $e$ -folding time of  $O(10^2)$  years is also found for clockwise rotated long bed waves when strong tidal currents and smaller values of the Coriolis parameter are considered.

If the tidal strength is fixed at  $U_0^* = 0.6 \text{ ms}^{-1}$  and the ellipticity is varied, both clockwise and counterclockwise long bed waves form when  $e$  is larger than about 0.2, up to almost circular tides. Finally, runs have been made using the sediment transport rate formulations of Meyer-Peter & Muller (1948) and Soulsby and Van Rijn (Soulsby 1997) instead of that proposed by Fredsøe & Deigaard (1992). The differences in  $k$  and  $\alpha$  of the fastest growing modes are negligible, even though the  $e$ -folding time becomes a factor 2 and 30 longer, respectively. For  $\theta$  tending to  $\theta_c$  the sediment transport rate calculated with Fredsøe & Deigaard's formula (Fredsøe & Deigaard 1992) tends to vanish as  $\theta - \theta_c$  while the value of  $Q$  predicted by means of Meyer-Peter and Muller, and Soulsby and Van Rijn's formulae tends to zero as  $(\theta - \theta_c)^{3/2}$  and  $(\sqrt{\theta} - \sqrt{\theta_c})^{2.4}$ , respectively. The use of a different sediment transport formulae only enhances or reduces the growth of the bedforms.

## 5. Conclusions

A simple model has been developed and analysed to explain the appearance of the long bed waves revealed by the field surveys carried out at the Noordhinder area (North Sea). The theoretical results obtained provide not only a physical explanation of the mechanism originating long bed waves, but also yields quantitative information about the geometrical characteristics of these bottom patterns. A necessary element to model long bed waves is that the sediment transport formulation includes a critical bottom stress of erosion. Moreover, long bed waves are obtained in the case that tidal currents are elliptical, and weak, in the sense that their maximum stress exerted

at the bottom is slightly above the critical stress of erosion. A sensitivity analysis of the model results with respect to changes of the parameters shows that the model findings are quite robust.

A qualitative comparison of the model results with field data supports the model findings, but further refinements of the model (e.g. the deviation  $\phi$  of the bed shear stress from the direction of the depth-averaged velocity should be accounted for Shapiro 2004) are required to obtain accurate quantitative predictions of bedform characteristics. If  $\phi$  is accounted for by means of an empirical approach (i.e. assuming  $\phi = 10^\circ$ ) and the values of the parameters slightly tuned, a significant improvement of the model results is achieved and the angle formed by the crests of the second mode with the major axis of the tidal ellipse turns out to be about  $-45^\circ$ . Moreover, while the incorporation of  $\phi$  improves the prediction of the geometrical characteristics of the counterclockwise modes, it does not significantly affect those of the clockwise rotated modes. Of course, only a full three-dimensional approach can provide a reliable evaluation of the angle  $\phi$  which should depend on the tidal phase.

The authors wish to thank Dr Thaiënne van Dijk (TNO/Deltares, Utrecht) who kindly provided a first version of her analysis of the field data, and also helped to improve an earlier version of this manuscript.

#### REFERENCES

- BESIO, G., BLONDEAUX, P. & VITTORI, G. 2006 On the formation of sand waves and sand banks. *J. Fluid Mech.* **557**, 1–27.
- CARBAJAL, N. 1997 Two application of Taylor's problem solution for finite rectangular semi-enclosed basins. *Cont. Shelf Res.* **17** (7), 803–817.
- FREDSØE, J. & DEIGAARD, R. 1992 *Mechanics of Coastal Sediment Transport*. World Scientific.
- HULSCHER, S. J. M. H., DE SWART, H. E. & DE VRIEND, H. J. 1993 The generation of offshore tidal sand banks and sand waves. *Cont. Shelf Res.* **13**, 1183–1204.
- HUTHNANCE, J. M. 1982 On one mechanism forming linear sand banks. *Est. Coast. Shelf Sci.* **14**, 79–99.
- KNAAPEN, M. A. F. 2008 Sandbank occurrence on the Dutch continental shelf in the North Sea. *Geo-Mar. Lett.* **29**, 17–24. DOI: 10.1007/s00367-008-0105-7.
- KNAAPEN, M. A. F., HULSCHER, S. J. M. H., DE VRIEND, H. J. & STOLK, A. 2001 A new type of sea bed waves. *Geophys. Res. Lett.* **28** (7), 1323–1326.
- KOVACS, A. & PARKER, G. 1994 A new vectorial bedload formulation and its application to the time evolution of straight river channel. *J. Fluid Mech.* **267**, 153–183.
- MEYER-PETER, E. & MULLER R. 1948 Formulas for bed-load transport. In *Proceedings of the Second Meeting, International Association for Hydraulic Structures Research*, Stockholm, Sweden.
- RICHARDS, K. J. 1980 The formation of ripples and dunes on an erodible bed. *J. Fluid Mech.* **99**, 597–618.
- SEMINARA, G. 1998 Stability and morphodynamics. *Meccanica* **33**, 59–99.
- SHAPIRO, G. I. 2004 A 2.5D model for sand transport in a shallow sea: effect of Ekman veering. *Cont. Shelf Res.* **24**, 659–671.
- SOULSBY, R. L. 1997 *Dynamics of Marine Sands*. Thomas Telford.
- SOULSBY, R. L. & WHITEHOUSE R. J. S. 2005 Prediction of ripple properties in shelf seas. Mark 2 predictor for time evolution. *Tech. Rep.* TR155 Release 2.0, HR Wallingford Ltd, UK.
- TALMON, A. M., STRUKSMA, N. & VAN MIERLO, M. C. L. M. 1995 Laboratory measurements of the direction of sediment transport on transverse alluvial-bed slopes. *J. Hydraul. Res.* **33**, 495–517.